

Cavity ring-down Faraday rotation spectroscopy for oxygen detection

Jonas Westberg¹  · Gerard Wysocki¹

Received: 31 January 2017 / Accepted: 7 May 2017 / Published online: 13 May 2017
© Springer-Verlag Berlin Heidelberg 2017

Abstract A combination of the path length enhancement provided by cavity ring-down spectroscopy together with the selectivity and noise suppression capabilities of Faraday rotation spectroscopy is utilized for highly sensitive detection of oxygen at ~ 762.3 nm. The system achieves a noise-equivalent rotation angle of 1.3×10^{-9} rad/ $\sqrt{\text{Hz}}$, and a trace O₂ detection limit of 160 ppb for 100 s of averaging. The technique relies on measurements of the losses in two orthogonal polarization directions simultaneously, whereby an absolute assessment of the magnetically induced polarization rotation can be retrieved, analogous to the absolute absorption measurement provided by stand-alone cavity ring-down spectroscopy. The differential nature of the technique described here eliminates the need for off-resonance decay measurements and thereby allows for efficient shot-to-shot fluctuation suppression. This is especially advantageous when operating the system under measurement conditions that severely affect the non-absorber related losses, such as particulate matter contamination typically present in combustion or open-path applications.

1 Introduction

Oxygen (O₂) plays a vital role in the ecosystem and reliable assessments of the concentrations of oxygen are

paramount for an accurate description of many important environmental, biological, and geochemical processes [1–3]. In addition, oxidation can have costly consequences in various high-tech fields, such as the semiconductor- or the pharmaceutical industries. As these technologies progress, more stringent demands are imposed on the involved trace oxygen sensing systems, with higher accuracy, robustness, and faster response times. For these reasons, highly sensitive and non-invasive, in situ oxygen sensors are needed to actively monitor the concentration levels of O₂ without suffering from systematic drifts or require frequent re-calibration. Electrochemical oxygen sensors have been used extensively in the past [4, 5], but these systems are prone to drifts and often depend on recurring calibration procedures. The direct measurement capabilities provided by the laser-based optical sensors seem promising in this regard, and several laser-based techniques have been explored to date. These include tunable-diode laser spectroscopy (TDLAS), quartz-enhanced photoacoustic spectroscopy (QEPAS), cavity-enhanced absorption spectroscopy (CEAS), and Faraday rotation spectroscopy (FRS) [6–15]. However, these techniques often struggle to reach the desired minimum detection limits (<ppmv), or are subject to optical fringes and drifts, which limit their maximum averaging times and consequently the achievable ultimate detection limits. In this work, the molecular interaction length enhancement provided by a high-finesse cavity is leveraged together with a balanced detection polarimetric scheme provided by Faraday rotation spectroscopy to achieve high-sensitivity oxygen detection. The proposed system utilizes the quantitative properties of cavity ring down spectroscopy (CRDS) to probe the polarization rotation induced by the oxygen molecules, while the balanced polarimetric detection provides effective suppression of non-oxygen related losses in the cavity (e.g. induced by particulate matter contamination).

This article is part of the topical collection “Field Laser Applications in Industry and Research” guest edited by Francesco D’Amato, Erik Kerstel, and Alan Fried.

✉ Gerard Wysocki
gwysocki@princeton.edu

¹ Department of Electrical Engineering, Princeton University, Princeton, NJ 08544, USA

1.1 Faraday rotation spectroscopy

Faraday rotation spectroscopy is a laser-based magneto-optical technique for sensitive and selective detection of paramagnetic gaseous species (e.g. O_2 , NO, NO_2 , OH, HO_2) [7, 16–19]. The technique relies on the Faraday effect (magnetically induced circular birefringence), which occurs for light that is resonant with optical transitions of paramagnetic species exposed to an external magnetic field. The Faraday effect introduces a rotation of the plane of polarization of linearly polarized light, which is proportional to the number density of the interacting paramagnetic molecules. The subtle change in the polarization state of the light is converted to an intensity change by introducing a polarization-selective element (analyzer) prior to the photodetector. Spectroscopic dispersion information from the sample species is by this procedure encoded in the photodetector response signal, which can be used for quantitative concentration assessments.

The sensitivity enhancement of FRS compared to corresponding conventional TDLAS-based techniques arises mainly from its noise suppression properties [17–19]. In particular, large suppression of intensity noise from the laser source usually observed in TDLAS is made possible by high extinction ratio polarizers. Furthermore, the magnetic field and/or the laser wavelength can be modulated, which encodes the polarization rotation signal at higher frequencies where experimental $1/f$ noise (flicker noise) is substantially reduced. The FRS signal can be retrieved by phase sensitive detection (e.g. by a lock-in amplifier) at harmonics of the modulation frequency. The polarization signal can also be detected using balanced optical detection, which suppresses common mode laser intensity noise measured by the two detectors. Also, direct modulation of the sample response through control of the magnetic field can significantly reduce noise associated with optical fringes, which is often a limiting factor for absorption-based laser spectroscopy. These noise suppression techniques have enabled FRS systems that operate near the quantum shot noise limit [20, 21]. Once this fundamental limit is achieved, only methods that increase the FRS signal can lead to further improvements in system sensitivity, and thus cavity-enhancement is studied in this work.

1.2 Cavity ring-down spectroscopy

Cavity ring-down spectroscopy [22, 23] is a cavity-enhanced absorption technique that has demonstrated excellent performance [24] with noise-equivalent absorptions (NEAs) only rivaled by the noise-immune cavity-enhanced optical-heterodyne molecular spectroscopy (NICE-OHMS) technique [25]. A schematic overview of a typical CRDS system is shown in Fig. 1. The technique

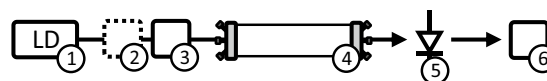


Fig. 1 Basic schematic of a cavity ring-down system. ① Laser operating in continuous wave mode, ② (optional) fast optical shutter, e.g. an acousto-optical modulator, ③ beam shaping optics, ④ high-finesse cavity assembly (possibly including piezo actuators for cavity length modulation), ⑤ measurement detector and electronics, ⑥ analog to digital conversion electronics and data processing

measures the intensity decay of light transmitted through a cavity as a function of laser frequency after a rapid interruption of the cavity injection. The decay rate measurement infers that the technique is inherently insensitive to intensity noise, which contributes to the low detection limits. However, it usually suffers from rather low duty cycle due to the time separation of acquired ring-down events.

CRDS provides an absolute measurement of the losses of the cavity, but to distinguish absorption losses induced by the absorbing species from general losses of the cavity (mirror losses, scattering from particles, etc.), an “empty cavity” or off-resonance measurement (τ_0) is performed at regular time intervals to maintain the system accuracy. This measurement can be performed by removing the sample species from the cavity (zero-gas measurement) or simply by detuning the frequency of the laser from the absorption transition of the molecules (off-resonance measurement). The calibration measurement time interval depends on the drifts of the system and a suitable calibration interval needs to be determined on system/application basis.

A combination of CRDS and FRS enables a differential measurement capability [26], which, similarly to saturated absorption cavity ring-down (SCAR) [27], does not require separate τ_0 measurements. This is achieved by comparing the intensity decay rates measured in two orthogonal polarization directions simultaneously. The FRS signal is encoded in the difference of the two decay rates, which share the same empty cavity ring-down time. Thus, the cavity ring-down Faraday rotation spectroscopy (CRD-FRS) signal is independent of τ_0 , which relieves the demand of recalibration and makes the system highly unsusceptible to τ_0 fluctuations, which are typically a characteristic of noisy measurement environments.

2 Cavity ring-down Faraday rotation spectroscopy

A general layout of CRD-FRS is shown in Fig. 2. It is based on a conventional CRDS setup with a couple of important additions: (1) components for polarization control are added to the beam path prior to the cavity to carefully define the polarization direction of the light injected into

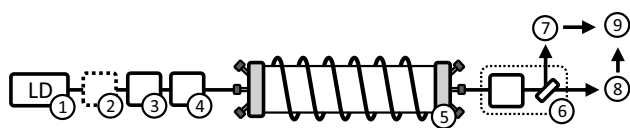


Fig. 2 General layout of the CRD-FRS setup. ① Laser operating in continuous wave mode, ② (optional) fast optical shutter, e.g. an acousto-optical modulator, ③ beam shaping optics, ④ polarization controlling optics, ⑤ high-finesse cavity and permanent magnet/solenoid for axial magnetic field (possibly including piezo actuators for cavity length modulation), ⑥ polarization analyzing optics to divide the light into two orthogonal polarizations, ⑦ measurement detector and electronics, ⑧ measurement detector and electronics, ⑨ analog to digital conversion electronics and data processing

the cavity, (2) a polarization-selective assembly is inserted after the cavity to enable the measurement of losses in the two orthogonal polarization directions, (3) an electromagnetic coil or permanent magnet assembly is added to the system to induce an axial magnetic field that interacts with the paramagnetic species along the optical axis of the cavity. When the frequency of the laser is scanned across the transition of a paramagnetic species subjected to the axial magnetic field, the Faraday effect will continuously transfer a fraction of the intra-cavity optical power from one polarization state to the other. Through this process, the losses measured by the ring-down decays on the two detectors will differ and the Faraday rotation induced by the molecules can be measured in an absolute sense. If a transverse magnetic field is used, the Voigt effect rather than the Faraday effect can be detected [6].

It is important to note that the data acquisitions for the two detector channels are triggered simultaneously and, therefore, the two detectors measure the intensity decay for the same ring-down event albeit in different polarization directions. The empty cavity ring-down time is thus equal in the two channels and can be cancelled. A differential detection method such as this has several advantages. First, as mentioned previously, there is no longer a requirement to perform frequent calibrations of the empty cavity/off-resonance ring-down time, which opens the possibility of true line locking to the peak of the transition of interest. This also implies that the system will be insensitive to fluctuations of additional losses (losses that do not contribute to the polarization rotation). Such losses can, for instance, occur under measurement conditions that contain a large number of particulate matter that interfere with the beam during the decay event (i.e. in an open-path cavity-enhanced systems). Second, the system will be insensitive to any fluctuating background due to spectrally interfering diamagnetic species (CO_2 , H_2O , etc.) that may be of concern when the absorption spectrum is measured by conventional CRDS. Third, the system measures the polarization rotation in an absolute sense, which opens the possibility of a calibration-free spectrometer.

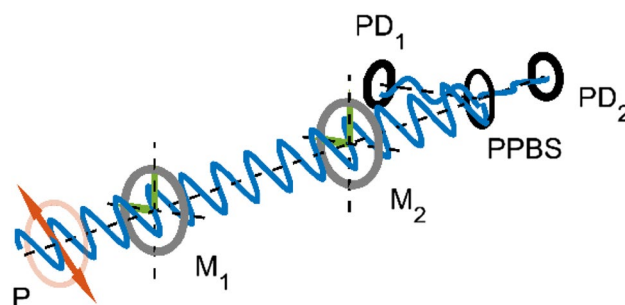


Fig. 3 Schematic overview of the electric field propagation in the CRD-FRS system. The polarization of the incoming light (P) is oriented at 45° with respect to the analyzer. Without polarization rotation, a perfect balance is maintained between the two optical powers impinging on the detectors. A magnetically induced polarization rotation continuously transfers power from one branch to the other, which gives rise to different losses and thus different ring-down times measured by the detectors. $M_{1,2}$ cavity mirrors, $PD_{1,2}$ photodetectors, $PPBS$ polarizing beam splitter used as the analyzer, B magnetic field vector

3 Theoretical description of cavity ring-down Faraday rotation spectroscopy

Faraday rotation spectroscopy signals can be conveniently described using the Jones matrix approach [28] and extensive theoretical descriptions have been published in the works by Müller et al. [29] and Dupré [30]. Here, a short derivation of the CRD-FRS signal is given for our particular experimental configuration.

For convenience, this analysis assumes that the incoming polarization direction is aligned at 45° with respect to the analyzer (see Fig. 3). The initial polarization state of the electric field after passing the polarizer is thus given by

$$E_i = \frac{E_0}{\sqrt{2}} \begin{bmatrix} 1 \\ 1 + i\varepsilon \end{bmatrix}, \quad (1)$$

where a small polarization ellipticity, ε , has been added to account for polarizer imperfections due to the finite extinction ratio of the polarizer [31]. The Jones matrix for a single round trip in the cavity is given by a matrix multiplication of the Jones' matrices of the individual components, i.e.

$$J_{\text{tot}} = J_n J_{n-1} \dots J_2 J_1. \quad (2)$$

The light inside a cavity of length L will experience an attenuation and a phase shift due to magnetic circular dichroism (MCD) and magnetic circular birefringence (MCB), whose Jones' matrices can be written as

$$J_{\text{MCD}} = e^{-\alpha L/2} \begin{bmatrix} \cos h(\Delta\alpha L/4) & i \sin h(\Delta\alpha L/4) \\ -i \sin h(\Delta\alpha L/4) & \cos h(\Delta\alpha L/4) \end{bmatrix}, \quad (3)$$

and

$$J_{\text{MCB}} = \begin{bmatrix} \cos(\Delta n L \pi / \lambda) & -\sin(\Delta n L \pi / \lambda) \\ \sin(\Delta n L \pi / \lambda) & \cos(\Delta n L \pi / \lambda) \end{bmatrix}, \tag{4}$$

respectively, where $\alpha = \alpha_R + \alpha_L$, $\Delta\alpha = \alpha_R - \alpha_L$, and $\Delta n = n_R - n_L$ is the total absorption, the difference in absorption, and the difference in refractive index between right-hand and left-hand circularly polarized light components. The Jones' matrices for the cavity mirrors (here assumed to be identical) are given by

$$J_{\text{MIR}} = \sqrt{R} \begin{bmatrix} -1 & 0 \\ 0 & 1 \end{bmatrix}, \tag{5}$$

where R is the reflectivity of the mirrors. The Jones' matrix for a round-trip in the cavity will be given by,

$$J_{\text{rt}} = J_{\text{MCD}} J_{\text{MCB}} J_{\text{MIR}} J_{\text{MCB}} J_{\text{MCD}} J_{\text{MIR}}, \tag{6}$$

$$J_{\text{rt}} = R e^{-\alpha L / 2} \begin{bmatrix} \cos h\left(\frac{\Phi}{2} + i\Theta\right) & i \sin h\left(\frac{\Phi}{2} + i\Theta\right) \\ -i \sin h\left(\frac{\Phi}{2} + i\Theta\right) & \cos h\left(\frac{\Phi}{2} + i\Theta\right) \end{bmatrix}, \tag{7}$$

where the differential absorption, $\Phi = \Delta\alpha L / 2$, and the Faraday rotation angle, $\Theta = \Delta n L \pi / (2\lambda)$, have been introduced. The total Jones' matrix after N round-trips is given by

$$J_{\text{tot}} = (J_{\text{rt}})^N,$$

$$J_{\text{tot}} = R^N e^{-N\alpha L / 2} \begin{bmatrix} \cos h\left(\frac{N\Phi}{2} + iN\Theta\right) & i \sin h\left(\frac{N\Phi}{2} + iN\Theta\right) \\ -i \sin h\left(\frac{N\Phi}{2} + iN\Theta\right) & \cos h\left(\frac{N\Phi}{2} + iN\Theta\right) \end{bmatrix}, \tag{8}$$

where it is assumed that $N \gg 1$. The electric field directly after the cavity is given by

$$E_f = J_a J_{\text{tot}} E_i, \tag{9}$$

where J_a is the Jones' matrix for the analyzer given by

$$J_a = \begin{bmatrix} a \sin^2(\phi) & a \sin(\phi) \cos(\phi) \\ +b \cos^2(\phi) & -b \sin(\phi) \cos(\phi) \\ a \sin(\phi) \cos(\phi) & a \cos^2(\phi) \\ -b \sin(\phi) \cos(\phi) & +b \sin^2(\phi) \end{bmatrix}, \tag{10}$$

where ϕ is the analyzer angle (with respect to the first polarizer) and $a \approx 1$ and $b \ll a$ represents polarization imperfections due to the finite extinction ratio of the analyzer. This means that the intensities for the s- and p-polarizations (up to 2nd order terms) are given by

$$I_s = \frac{I_0}{4} e^{-t/\tau_0} e^{-t/\tau} \left[2(a^2 + b^2) \cos h\left(\frac{c\Phi t}{2L}\right) + 2a^2 \sin\left(\frac{c\Theta t}{L} + 2\phi\right) - (2b^2 - \varepsilon^2 a^2) \cos\left(\frac{c\Theta t}{L} + 2\phi\right) - 2\varepsilon a^2 \sin h\left(\frac{c\Phi t}{2L}\right) + a^2 \varepsilon^2 \cos h\left(\frac{c\Phi t}{2L}\right) \right], \tag{11}$$

and

$$I_p = \frac{I_0}{4} e^{-t/\tau_0} e^{-t/\tau} \left[2(a^2 + b^2) \cos h\left(\frac{c\Phi t}{2L}\right) - 2a^2 \sin\left(\frac{c\Theta t}{L} + 2\phi\right) + (2b^2 - \varepsilon^2 a^2) \cos\left(\frac{c\Theta t}{L} + 2\phi\right) - 2\varepsilon a^2 \sin h\left(\frac{c\Phi t}{2L}\right) + a^2 \varepsilon^2 \cos h\left(\frac{c\Phi t}{2L}\right) \right], \tag{12}$$

respectively, where a variable substitution, $N \rightarrow t/t_{\text{rt}} = ct/(2L)$, from the number of round-trips into the corresponding time has been performed, which is easily accomplished by considering the time it takes to make a single round-trip, t_{rt} . Also, the reflectivity R is rewritten using the empty cavity ring-down time, τ_0 ,

$$\tau_0 = \frac{L}{c|\ln R|}, \tag{13}$$

$$\Rightarrow R^{2N} = e^{-t/\tau_0},$$

and a ring-down time due to the non-mirror related losses in the cavity, τ , is introduced. The expressions given in Eqs. (11) and (12) can be simplified further by assuming decent polarizers (extinction ratio >1000:1), i.e. $a \approx 1$, $b \ll a$, and $\varepsilon \ll 1$. This means that Eqs. (11) and (12) can be reduced to

$$I_s = \frac{I_0}{2} e^{-t/\tau_0} e^{-t/\tau} \left[\cos h\left(\frac{c\Phi t}{2L}\right) + \sin\left(\frac{c\Theta t}{L} + 2\phi\right) - \varepsilon \sin h\left(\frac{c\Phi t}{2L}\right) \right], \tag{14}$$

and

$$I_p = \frac{I_0}{2} e^{-t/\tau_0} e^{-t/\tau} \left[\cos h\left(\frac{c\Phi t}{2L}\right) - \sin\left(\frac{c\Theta t}{L} + 2\phi\right) - \varepsilon \sin h\left(\frac{c\Phi t}{2L}\right) \right]. \tag{15}$$

It is easy to see that if there is no magnetic field, i.e. $\Phi = 0$ and $\Theta = 0$ the expressions reduce to the expected ring-down decays for conventional cavity ring-down spectroscopy. By introducing a magnetic field the decays of each polarization start to oscillate as determined by the terms in the brackets of Eqs. (14) and (15).

From these equations, it can be concluded that polarizer imperfections of the initial polarizer (ε) couple magnetic circular dichroism (MCD) contributions to the intensity decays to the first order, whereas imperfections of the analyzer (a and b) only appear in second-order terms. Furthermore, the MCD contributions in the two orthogonal polarization directions are of the same sign and will thus contribute equally to

the overall losses in the two polarization directions, which may be conveniently cancelled via differential measurements. It is now appropriate to consider only cases where the overall magnetic circular birefringence and dichroism are small. This leads to additional simplifications of Eqs. (14) and (15) yielding

$$I_s \approx \frac{I_0}{2} e^{-t/\tau_0} e^{-t/\tau} \left[1 + \left(\frac{c\Theta t}{L} \right) \cos(2\phi) + \sin(2\phi) - \varepsilon \left(\frac{c\Phi t}{2L} \right) \right], \tag{16}$$

and

$$I_p \approx \frac{I_0}{2} e^{-t/\tau_0} e^{-t/\tau} \left[1 - \left(\frac{c\Theta t}{L} \right) \cos(2\phi) - \sin(2\phi) - \varepsilon \left(\frac{c\Phi t}{2L} \right) \right], \tag{17}$$

where the angle sum identity for the sine function has also been used. These expressions can be re-written as single exponential decays,

$$I_s \approx \frac{I_0}{2} \exp \left\{ -\frac{t}{\tau_0} - \frac{t}{\tau} - t \left[\left(\frac{c\Theta t}{L} \right) \cos(2\phi) - \varepsilon \left(\frac{c\Phi t}{2L} \right) + \sin(2\phi) \right] \right\}, \tag{18}$$

$$I_p \approx \frac{I_0}{2} \exp \left\{ -\frac{t}{\tau_0} - \frac{t}{\tau} - t \left[-\left(\frac{c\Theta t}{L} \right) \cos(2\phi) - \varepsilon \left(\frac{c\Phi t}{2L} \right) - \sin(2\phi) \right] \right\}, \tag{19}$$

which leads to the following expression for the decay times in the two orthogonal polarizations,

$$\frac{1}{\tau_s} \approx \frac{1}{\tau_0} + \frac{1}{\tau} + \left(\frac{c\Theta}{L} \right) \cos(2\phi) - \varepsilon \left(\frac{c\Phi}{2L} \right), \tag{20}$$

$$\frac{1}{\tau_p} \approx \frac{1}{\tau_0} + \frac{1}{\tau} - \left(\frac{c\Theta}{L} \right) \cos(2\phi) - \varepsilon \left(\frac{c\Phi}{2L} \right), \tag{21}$$

This shows that the Faraday rotation induced by the paramagnetic molecules manifests itself as either an additional decrease or as an additional increase in the ring-down times (1st order approximation). Figure 4 shows a numerical simulation of the intensity decays in the two orthogonal polarization directions based on the theoretical model described above. The additional gain and loss introduced by the Faraday rotation is clearly visible in the two detector channels. The intensity decay of conventional CRDS has been added as a reference.

It follows that the difference in decay times can be written as

$$\frac{1}{\tau_s} - \frac{1}{\tau_p} = 2 \left(\frac{c\Theta}{L} \right) \cos(2\phi), \tag{22}$$

which implies that the Faraday rotation signal can be succinctly written as

$$\Theta = \frac{L \cos(2\phi)}{2c} \left(\frac{1}{\tau_s} - \frac{1}{\tau_p} \right). \tag{23}$$

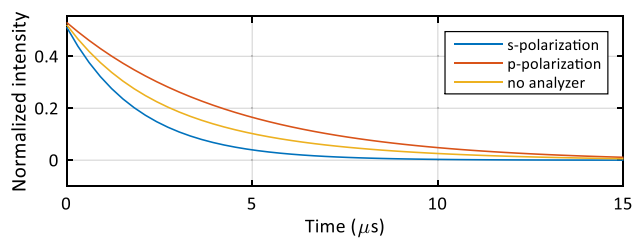


Fig. 4 Plot of a numerical calculation of intensity decays in the two orthogonal polarization directions. The s- and p-polarization decays are represented by the blue and red traces, respectively. The intensity decay of conventional CRDS (without analyzer) is introduced as a reference (yellow trace). The Faraday rotation induced gain and loss in the two detection channels are clearly visible

From Eq. (23) it can be concluded that the maximum Faraday rotation signal occurs for analyzer angles, $\phi = k\pi/2$, where $k = 0, 1, 2, \dots$, i.e. oriented at either 0° or 90° . Since the initial polarization was oriented at 45° , this

analyzer configuration divides the light equally in terms of initial intensities. It should be noted that minor deviations from the optimum angle will have negligible impact on the measurement precision (2nd order effect) and no particular emphasis need to be placed on careful analyzer angle optimization (unlike conventional 90° -method Faraday rotation spectroscopy, which requires precise analyzer offset angle adjustment). This result is consistent with that reported by Dupré [30] and Müller et al. [29, 32], but differs from that derived by Engeln et al. [26] by a factor of $1/[\cos(2\phi) \sin(2\phi)]$, which likely stems from an incorrect treatment of the electric field transmitted through the analyzer (see Eq. A11 in [26]). Small values of ϕ would in this case yield unrealistically large rotations as $\Theta \rightarrow \infty$ when $\phi \rightarrow 0$.

3.1 Comparison between CRDS and CRD-FRS ring-down measurements

A simple error propagation calculation can be performed to compare the expected performance of CRDS and CRD-FRS under the assumption that they possess similar decay time distributions (i.e. they operate under the same measurement conditions). For convenience, the minimum detectable absorption is used as the metric of comparison. In conventional CRDS the absorption is given by [22]

$$\alpha L = \frac{L}{c} \left(\frac{1}{\tau} - \frac{1}{\tau_0} \right). \tag{24}$$

Assuming a standard deviation of the ring-down decays, σ_τ , the propagation of uncertainty in Eq. (24), which contains two ring down measurements with uncorrelated noise, yields an absorption uncertainty of

$$\sigma_{\alpha L} = \frac{L}{c} \sqrt{\frac{\sigma_\tau^2}{\tau^4} + \frac{\sigma_\tau^2}{\tau_0^4}}. \tag{25}$$

For CRD-FRS, the ring down decays for both polarizations are measured simultaneously and can, therefore, be highly correlated. In this case, the propagation of uncertainty with correlated variables gives

$$\sigma_\Theta = \frac{L}{2c} \sqrt{\frac{\sigma_\tau^2}{\tau_s^4} + \frac{\sigma_\tau^2}{\tau_p^4} - \frac{2\rho\sigma_\tau^2}{\tau_s^2\tau_p^2}}, \tag{26}$$

where ρ is the correlation coefficient between s- and p-polarization decays measured for the same ring-down event. Close to the detection limit, where the absorption is small, the decay times in the above equations are approximately equal, i.e. $\tau_s \approx \tau_p \approx \tau_0 \approx \tau$. Equation (25) and (26) then simplify to

$$\sigma_{\alpha L} = \frac{\sqrt{2}L}{c} \frac{\sigma_\tau}{\tau^2}, \tag{27}$$

and

$$\sigma_\Theta = \frac{\sqrt{2}L}{2c} \frac{\sigma_\tau}{\tau^2} \sqrt{1 - \rho}, \tag{28}$$

respectively. In order to relate the two quantities we utilize the approximation relating Θ and $(\alpha L)_{\min}$ in a dilute medium [33], which gives an equivalent absorption in FRS of $\sigma_{\alpha L-\Theta} \cong 4\sigma_\Theta$. In order to compare the two techniques we solve for a ratio of $\sigma_{\alpha L-\Theta}$ and $\sigma_{\alpha L}$, which gives

$$\frac{\sigma_{\alpha L}}{\sigma_{\alpha L-\Theta}} = \frac{1}{2\sqrt{1 - \rho}}. \tag{29}$$

From the equation above it is clear that if the CRD-FRS system is affected by uncorrelated noise in the two polarization channels (e.g. detector or shot noise), the measurement precision will be two times worse than in the corresponding CRDS system. However, in the case of correlated noise (e.g. due to particle scattering) the CRD-FRS system can significantly improve the precision. At a correlation coefficient of 0.75 the techniques show similar performance, and for correlation coefficients of 0.94–0.99 the CRD-FRS is expected to yield a 2–5 times improvement. It is important to note that there is an upper limit on the correlation coefficient set either by the shot-noise or detector noise of the system. This prevents unrealistically large

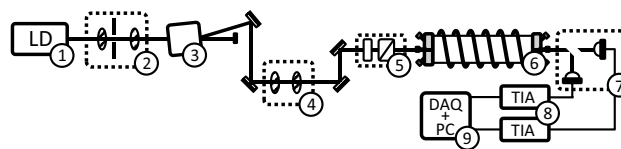


Fig. 5 Detailed schematic of the experimental setup for the CRD-FRS system designed for this project. ① Laser operating in continuous wave mode, ② spatial filter comprising two lenses and a pinhole, ③ acousto-optical modulator (AOM), ④ mode-matching optics, ⑤ injection polarization controller (half waveplate and linear polarizer), ⑥ high-finesse cavity and solenoid, ⑦ plate polarizing beamsplitter and two photodetectors, ⑧ matched transimpedance amplifiers (FEMTO DHCP-100), ⑨ DAQ-card and PC for data collection and numerical processing

improvement factors for CRD-FRS. Also note that this simplified scenario does not consider any additional qualities of the FRS techniques such as the improved immunity to interfering diamagnetic species or optical fringe suppression through magnetic field modulation.

4 Experimental method and procedures

The cavity ring-down Faraday rotation spectrometer developed in this work is schematically shown in Fig. 5. It is based on a diode laser from Sacher Lasertechnik (Cheetah) operating at 762 nm, which was chosen due to its relatively high output power (30 mW) and its ability to target the $^3P_1(1)$ transition of oxygen in the A electronic band, which exhibits the greatest susceptibility to the magnetic field strengths typically reachable with solenoids of practical size and reasonable power consumption (150–300 Gauss at 50 W). The technique was also tested using a set of cylindrical permanent neodymium magnets (axially magnetized) arranged in an octupole configuration [7]. The permanent magnets allow for unobstructed flow and continuous operation without power consumption, which is generally preferred for open-path cavity arrangements. However, this configuration lacks the convenience of field strength control provided by the DC-solenoid.

The emitted laser light was spatially filtered through a pinhole (Thorlabs, KT310) in order to produce a uniform Gaussian beam, which was then transmitted through an acousto-optical modulator (AOM). The AOM fulfills the role of the optical shutter in this system by shifting the direction of the beam and thereby rapidly interrupting the optical injection to the cavity.

The cavity assembly was constructed around a stainless-steel tube of 0.5 m length (CRD Optics, Inc.). Cavity mirror mounts were attached on either side of the stainless-steel tube using vacuum flanges. The tilt of the

mirrors was controlled through micrometer adjusters, of which one side used piezo-controlled actuators to allow for repeated cavity injection. In order to obtain a controllable magnetic field along the optical axis of the cavity, a solenoid was custom engineered to match the inner diameter of the tube. The solenoid was 25 cm in length with an inner and outer diameter of 0.5 and 1.5 inches, respectively. The length of the solenoid was chosen to not obstruct the flow through the cavity, which limited its length to roughly half of the cavity length. The magnetic field strength was controlled through the current provided by a DC power supply, which enabled continuous operation at approximately 300 Gauss of axial magnetic field using <40 W of power.

Prior to entering the cavity, the Gaussian beam was mode-matched to the cavity by two lenses placed at appropriate distances and the polarization direction of the light was rotated and filtered by a half-wave plate and a linear nanoparticle polarizer. The light transmitted through the cavity was divided into two orthogonal polarization directions by a polarizing plate beam-splitter before focusing on the photodetector surfaces. The photodetector currents were amplified by two similar transimpedance amplifiers (FEMTO DHPCA-100) before A/D conversion by a 16-bit, 200 MS/s DAQ-card (Gage Applied, FCiX Razor).

4.1 Mirror birefringence characterization

It is important to carefully characterize the polarization properties of the cavity mirrors to optimize the conditions for CRD-FRS. Mirror birefringence in the order of micro-radians will give rise to an offset of the CRD-FRS signal unless modulation of the magnetic field can be applied. Even state-of-the-art high reflectivity mirror coatings have shown to contain residual birefringence in the order of micro-radians per reflection [34–39]. Moreover, strain due to the mounting of the mirrors may introduce additional birefringence in the coatings. Any cavity birefringence that is not induced by the paramagnetic species may contribute to a small offset of the Faraday rotation signal. This offset can be remedied by co-aligning the fast and slow axis of the cavity mirror pair. A few different cavity mirror birefringence measurement procedures based on CRDS have been proposed in the literature [34, 36, 40]. They typically involve a rotation of one of the mirrors with respect to the other while the losses in a particular polarization direction are characterized.

Characterization of the cavity mirror birefringence of the two mirrors can be accomplished in a straightforward fashion using the CRD-FRS methodology. A zero-gas polarization rotation measurement is performed for different angular rotations of the cavity mirrors. One mirror remains

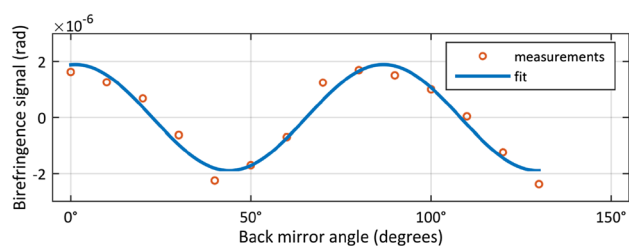


Fig. 6 Cavity mirror birefringence measurements as a function of back mirror angle. The figure shows the characteristics for one of the mirrors used as back mirror. Based on the measurements the two mirrors can be aligned in order to minimize the effects of linear cavity birefringence and polarization dependent losses when no Faraday rotation is present. The measurement shows a maximum birefringence contribution in the order of a few micro-radians

fixed while the other is gradually rotated around the optical axis of the cavity. The results from a set of such measurements are shown in Fig. 6. This information can be used to align the slow and fast axis of the two mirrors. By setting the mirrors at the zero-crossings of the curve in Fig. 6, the mirror axes are aligned and the effects of birefringence that cause the Faraday signal offset are suppressed. It is important to note that this procedure is not necessary if a modulation of the magnetic field is applied, which effectively nulls any constant offset in the Θ measurement.

5 Cavity ring-down Faraday rotation measurements of oxygen

The system was evaluated by measuring atmospheric oxygen under low pressure conditions with a closed-cavity. The spectroscopic data were acquired through stepping the injection current of the laser in increments of 100 μ A and cavity ring-down events were continuously collected at a rate of \sim 1 kHz for 50 ms per laser current step. The decays were analyzed offline by least square fitting to a standard model of the intensity decay, using the amplitude, decay time, and offset as free-parameters [41]. The off-resonance decay time was \sim 25 μ s. The two detector channels were analyzed separately and the results were used to calculate the CRD-FRS signal according to the theoretical model described in this work. The major isotope oxygen transition targeted was the $^{\text{P}}\text{P}_1(1)$ transition in the A electronic band around 762.3 nm and the sample pressure was set at \sim 8 Torr.

Figure 7 shows the absorption and Faraday rotation spectra obtained by stepping the injection current of the laser across the transition. Each measurement point represents intensity decay data acquired during a total acquisition time of 50 ms.

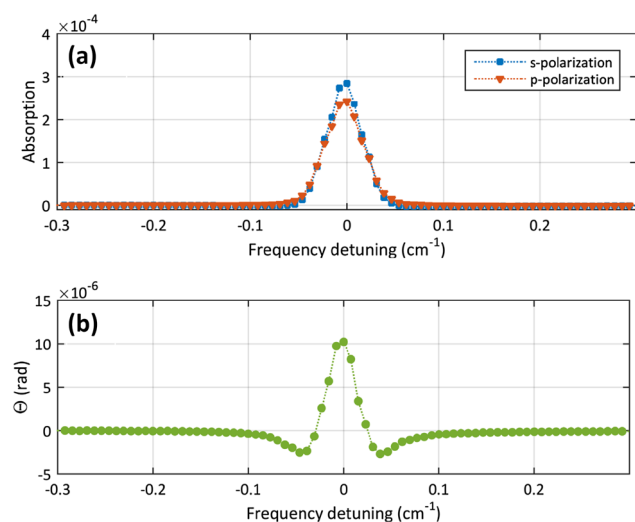


Fig. 7 **a** Absorption measurements for the two orthogonal polarization directions measured at 8 Torr of pressure. The difference in the losses experienced by the two polarizations is visible on the wings and at the peak of the absorption transition. **b** The corresponding CRD-FRS signal

6 Spectrometer performance and limitations

6.1 Shot-to-shot fluctuations

One of the main strengths of CRD-FRS is drawn from its ability to cancel fluctuations of non-absorber related losses that are often significant contributors of noise in conventional CRDS systems. Such additional losses may originate from micrometer sized particles passing through the cavity beam path or spatial inhomogeneities of the high reflectivity mirror coatings, which transforms vibrationally induced beam steering into fluctuations of the cavity losses. The differential nature of the CRD-FRS measurements can effectively suppress the influence of these noise sources since the non-absorber related losses are highly correlated in the two detector channels. To visualize this phenomenon, off-resonance measurements were recorded for the two detector channels in an open-path cavity configuration. Here, the stainless sample cell was removed and the solenoid replaced by permanent magnets (K&J magnetics, Inc., RX04X0) in an octupole magnet arrangement. This configuration was chosen to minimize the restriction of flow through the cavity. A total of 40 magnets were used, which resulted in a weight of 3.6 kg, comparable with the DC-solenoid weight. The results from this measurement are shown in Fig. 8 (vertical offsets have been added for visibility purposes). Solid lines represent smoothed data using Savitzky–Golay filter, which highlights the strong correlation between the two channels. By inspection of the solid lines it is clear

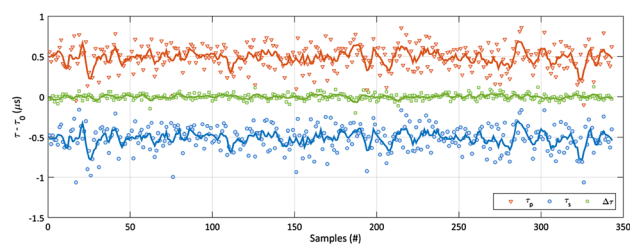


Fig. 8 Shot-to-shot fluctuations of off-resonance measurements in an open-path cavity configuration. The ring-down times for the s- and p-polarization have been vertically offset for visualization purposes. A *filtered solid line* has been added to the measurements in order to visualize the correlation between the data sets. The ring-down times in the two channels typically exhibit correlation coefficients $\rho > 0.9$, which is clearly observable when considering their difference (shown in the center)

that the two detector channels measure correlated losses. This gives rise to a significantly lower standard deviation of their difference shown as $\Delta\tau$, which is the basis for the Faraday rotation signal extraction. This cancellation of shot-to-shot fluctuations will be more pronounced for systems predominantly affected by this source of noise (e.g. open-path CRDS systems), while uncorrelated noise sources (e.g. detector noise) cannot be suppressed.

6.2 System stability

The stability of the system was evaluated by performing off-resonance Allan deviation [42] measurements using the open-path configuration that served as our worst-case laboratory conditions. The results from these measurements are displayed in Fig. 9. To demonstrate the effectiveness of the noise suppression properties discussed above, two Allan deviation measurements were performed under different noise conditions. Figure 9a shows the Allan deviation of a system that is severely affected by digitization noise from the data acquisition card (LeCroy 735Zi, 8-bit), which would be the equivalent of random detector noise. This type of noise is uncorrelated for the two polarization channels, which leads to an increase of the noise in the differential measurement ($\Delta\tau$) by $\sqrt{2}$ in the random-noise limited regime. It should be noted that at longer acquisition times, where the random noise component is averaged out and a system drift becomes dominant, the differential measurement shows visible improvement over the single channel measurement, which points to a correlated drift in both channels. The second measurement performed with a system with improved random noise characteristics resulted in the Allan deviation shown in Fig. 9b. In this measurement, the 8-bit DAQ-card was replaced with a 16-bit

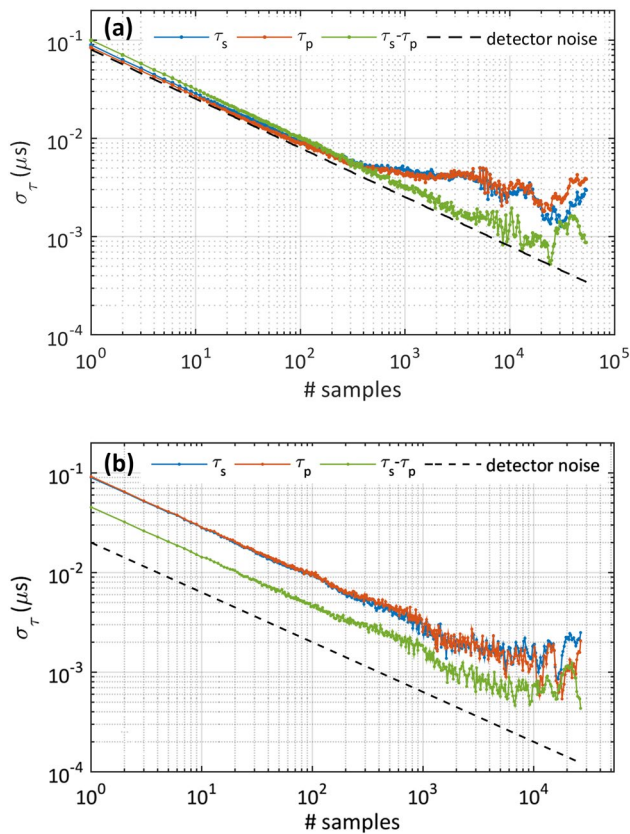


Fig. 9 Allan plots for two different detector noise levels. **a** The Allan deviation of a system that is limited by detector noise. Since this type of noise is not correlated between the two detector channels ($\rho < 0.01$), the CRD-FRS system exhibits a larger noise level compared to each individual channel. However, a slight improvement in long-term drift can be observed. **b** A system that is not limited by the detector noise. This uncovers the shot-to-shot fluctuations, which are highly correlated in the two detector channels

card, which results in significantly lower digitization noise affecting the intensity decay measurements. This uncovers the shot-to-shot fluctuations representing correlated noise in both channels with a correlation coefficient of $\rho = \sim 0.94$. An improvement by a factor of ~ 2 in the differential signal can be observed across all averaging times, which is consistent with Eq. (29).

6.2.1 Detection limit

The performance of the CRD-FRS spectrometer was estimated based on an off-resonance (baseline) measurement using the closed-cavity configuration with the DC-solenoid. The standard deviation of the Faraday rotation angle obtained by this measurement was $\sim 5.7 \times 10^{-9}$ rad, which yields a bandwidth-normalized noise-equivalent angle (NEA $_{\odot}$) of 1.3×10^{-9} rad/ $\sqrt{\text{Hz}}$. For direct comparison with other FRS systems it is more appropriate to cite

the cavity-length normalized NEA $_{\odot}$, which in case of our system (50 cm cavity) gives 2.6×10^{-11} rad/(cm $\sqrt{\text{Hz}}$). This is generally over an order of magnitude lower than previously reported values for short-path FRS spectrometers operating in the mid-IR spectral region [21, 43, 44] and in par with our best FRS systems for oxygen detection operating at the same wavelength and using a 6.8-m multi-pass cell [7, 20]. It should be noted, however, that while the multi-pass cell based system shows comparable short-term performance, over longer acquisition times these systems are strongly affected by system drift, and allowed only for averaging times in a 10- to 30-s range [7]. In contrast, the CRD-FRS system is white noise limited up to 10^3 s and provides a bandwidth-normalized minimum detection limit (MDL) for trace oxygen of 1.6 ppm/ $\sqrt{\text{Hz}}$ (estimated from the NEA $_{\odot}$ at an optimum operating pressure of 200 Torr and the available magnetic field of ~ 300 G). The system can reliably operate with 100 s integration time, which results in a trace oxygen detection limit of ~ 160 ppb.

7 Conclusion

A combination of cavity ring-down spectroscopy and Faraday rotation spectroscopy for sensitive oxygen detection has been experimentally implemented and theoretically described. This technique permits sensitive detection of paramagnetic gaseous species with improved detection limits under noisy measurement environments. The developed system relies on an enhancement of magneto-optical signals (Faraday effect demonstrated here or Voigt effect) by utilizing the large path length enhancement provided by a high-finesse optical cavity. An advantage of the technique is that it can be implemented into an existing cavity ring-down spectroscopy instrumentation by incorporating polarization-selective elements, an additional detector, and permanent magnets or an electromagnetic coil. The noise suppression qualities of Faraday rotation spectroscopy enables cavity-enhanced trace measurements of paramagnetic gases that can surpass what is possible with conventional cavity absorption spectroscopy under measurement conditions that are heavily contaminated by particulate matter, which introduces large fluctuations of non-absorber related cavity losses. Moreover, the CRD-FRS measurement builds on the strengths of the CRDS methodology and can offer an absolute measurement of the polarization rotation angle, which is a promising path to obtain calibration based on first principles linked to metrology standards. In addition, the technology can be adapted for detection of chiral molecules [29, 32, 45, 46] with only minor alterations of the experimental setup.

The CRD-FRS spectrometer presented in this work exhibits a NEA_{\odot} of 1.3×10^{-9} rad/ $\sqrt{\text{Hz}}$, which at optimum conditions can achieve trace oxygen detection limit of ~ 160 ppb for 100 s of integration time. Further opto-mechanical improvements of the cavity assembly, increased coil/cavity length ratio, active laser stabilization, and an increase in the system duty cycle, will enable a CRD-FRS spectrometer whose oxygen detection limit approaches tens of ppb levels.

Acknowledgements The authors gratefully acknowledge Marten Beels, Brian Siller, and Helen Waechter at Tiger Optics for useful discussions and insight regarding cavity ring-down spectroscopy. Financial support from the National Science Foundation (NSF) SECO EEC-1347523 Grant and CBET Grant #1507358 is also acknowledged.

References

1. X. Wang, O.S. Wolfbeis, Optical methods for sensing and imaging oxygen: materials, spectroscopies and applications. *Chem. Soc. Rev.* **43**, 3666–3761 (2014)
2. M. Quaranta, S.M. Borisov, I. Klimant, Indicators for optical oxygen sensors. *Bioanal. Rev.* **4**, 115–157 (2012)
3. Keeling, What atmospheric oxygen measurements can tell us about the global carbon cycle. *Glob. Biogeochem. Cycles* **7**, 37–67 (1993)
4. B.B. Stephens, P.S. Bakwin, P.P. Tans, R.M. Teclaw, D.D. Baumann, Application of a differential fuel-cell analyzer for measuring atmospheric oxygen variations. *J. Atmos. Ocean. Technol.* **24**, 82–94 (2007)
5. E.J. Morgan, J.V. Lavrič, T. Seifert, T. Chicoine, A. Day, J. Gomez, R. Logan, J. Sack, T. Shuuya, E.G. Ushona, K. Vincent, U. Schultz, E.-G. Brunke, C. Labuschagne, R.L. Thompson, S. Schmidt, A.C. Manning, M. Heimann, Continuous measurements of greenhouse gases and atmospheric oxygen at the Namib Desert Atmospheric Observatory. *Atmos. Meas. Tech.* **8**, 2233–2250 (2015)
6. L. Gianfrani, R.W. Fox, L. Hollberg, Cavity-enhanced absorption spectroscopy of molecular oxygen. *JOSA B* **16**, 2247–2254 (1999)
7. B. Brumfield, G. Wysocki, Faraday rotation spectroscopy based on permanent magnets for sensitive detection of oxygen at atmospheric conditions. *Opt. Express* **20**, 29727 (2012)
8. R.J. Brecha, L.M. Pedrotti, D. Krause, Magnetic rotation spectroscopy of molecular oxygen with a diode laser. *JOSA B* **14**, 1921–1930 (1997)
9. D.M. Brown, A.M. Brown, P.S. Edwards, Z. Liu, C.R. Philbrick, Measurement of atmospheric oxygen using long-path super-continuum absorption spectroscopy. *J. Appl. Remote Sens.* **8**, 083557 (2014)
10. X. Lou, G. Somesfalean, B. Chen, Z. Zhang, Oxygen measurement by multimode diode lasers employing gas correlation spectroscopy. *Appl. Opt.* **48**, 990–997 (2009)
11. D. Munzke, M. Böhm, O. Reich, Gaseous oxygen detection using hollow-core fiber-based linear cavity ring-down spectroscopy. *J. Light. Technol.* **33**, 2524–2529 (2015)
12. S. Neethu, R. Verma, S.S. Kamble, J.K. Radhakrishnan, P.P. Krishnapur, V.C. Padaki, Validation of wavelength modulation spectroscopy techniques for oxygen concentration measurement. *Sens. Actuators B Chem.* **192**, 70–76 (2014)
13. A. Pohlkötter, M. Köhring, U. Willer, W. Schade, Detection of molecular oxygen at low concentrations using quartz enhanced photoacoustic spectroscopy. *Sensors* **10**, 8466–8477 (2010)
14. M. Gupta, Highly-precise measurements of ambient oxygen using near-infrared cavity-enhanced laser absorption spectrometry. *Anal. Chem.* **84**, 7987–7991 (2012)
15. J. Hoffnagle, Measurement of atmospheric oxygen concentration by near-infrared absorption spectroscopy. American Geophysical Union, Fall Meeting, abstract A23E-0302 (2013)
16. A. Kaldor, W.B. Olson, A.G. Maki, Pollution monitor for nitric oxide: a laser device based on the zeeman modulation of absorption. *Science* **176**, 508–510 (1972)
17. G. Litfin, C.R. Pollock, R.F.C. Jr, F.K. Tittel, Sensitivity enhancement of laser absorption spectroscopy by magnetic rotation effect. *J. Chem. Phys.* **72**, 6602–6605 (1980)
18. R. Lewicki, J.H. Doty, R.F. Curl, F.K. Tittel, G. Wysocki, Ultra-sensitive detection of nitric oxide at 5.33 μm by using external cavity quantum cascade laser-based Faraday rotation spectroscopy. *Proc. Natl. Acad. Sci.* **106**, 12587–12592 (2009)
19. T.A. Blake, C. Chackerian, J.R. Podolske, Prognosis for a mid-infrared magnetic rotation spectrometer for the in situ detection of atmospheric free radicals. *Appl. Opt.* **35**, 973 (1996)
20. E.J. Zhang, B. Brumfield, G. Wysocki, Hybrid Faraday rotation spectrometer for sub-ppm detection of atmospheric O_2 . *Opt. Express* **22**, 15957 (2014)
21. Y. Wang, M. Nikodem, E. Zhang, F. Cikach, J. Barnes, S. Comhair, R.A. Dweik, C. Kao, G. Wysocki, Shot-noise limited Faraday rotation spectroscopy for detection of nitric oxide isotopes in breath, urine, and blood. *Sci. Rep.* **5**, 9096 (2015)
22. G. Berden, R. Engeln, *Cavity Ring-Down Spectroscopy: Techniques and Applications* (Wiley, Oxford, 2009)
23. G. Gagliardi, H.-P. Loock (eds.), *Cavity-Enhanced Spectroscopy and Sensing* (Springer, Berlin, 2014)
24. D.A. Long, A.J. Fleisher, S. Wójtciewicz, J.T. Hodges, Quantum-noise-limited cavity ring-down spectroscopy. *Appl. Phys. B* **115**, 149–153 (2014)
25. J. Ye, L.-S. Ma, J.L. Hall, Ultrasensitive detections in atomic and molecular physics: demonstration in molecular overtone spectroscopy. *J. Opt. Soc. Am. B* **15**, 6 (1998)
26. R. Engeln, G. Berden, E. van den Berg, G. Meijer, Polarization dependent cavity ring down spectroscopy. *J. Chem. Phys.* **107**, 4458–4467 (1997)
27. P. Cancio, I. Galli, S. Bartalini, G. Giusfredi, D. Mazzotti, P.D. Natale, Saturated-absorption cavity ring-down (SCAR) for high-sensitivity and high-resolution molecular spectroscopy in the Mid IR, in *Cavity-enhanced spectroscopy and sensing*, ed. by G. Gagliardi, H.-P. Loock (Springer, Berlin, 2014)
28. R.C. Jones, A new calculus for the treatment of optical systems VII properties of the N-matrices. *J. Opt. Soc. Am.* **38**, 671 (1948)
29. T. Müller, K.B. Wiberg, P.H. Vaccaro, J.R. Cheeseman, M.J. Frisch, Cavity ring-down polarimetry (CRDP): theoretical and experimental characterization. *JOSA B* **19**, 125–141 (2002)
30. P. Dupré, Birefringence-induced frequency beating in high-finesse cavities by continuous-wave cavity ring-down spectroscopy. *Phys. Rev. A* **92**, 053817 (2015)
31. R. Brecha, L. Pedrotti, Analysis of imperfect polarizer effects in magnetic rotation spectroscopy. *Opt. Express* **5**, 101–113 (1999)
32. T. Müller, K.B. Wiberg, P.H. Vaccaro, Cavity ring-down polarimetry (CRDP): a new scheme for probing circular birefringence and circular dichroism in the gas phase. *J. Phys. Chem. A* **104**, 5959–5968 (2000)
33. E. Zhang, Noise mitigation techniques for high-precision laser spectroscopy and integrated photonic chemical sensors. Princeton University, Princeton (2016)

34. H. Huang, K.K. Lehmann, Effects of linear birefringence and polarization-dependent loss of supermirrors in cavity ring-down spectroscopy. *Appl. Opt.* **47**, 3817–3827 (2008)
35. J.L. Hall, J. Ye, L.-S. Ma, Measurement of mirror birefringence at the sub-ppm level: proposed application to a test of QED. *Phys. Rev. A* **62**, 013815 (2000)
36. A.J. Fleisher, D.A. Long, Q. Liu, J.T. Hodges, Precision interferometric measurements of mirror birefringence in high-finesse optical resonators. *Phys. Rev. A* **93**, 013833 (2016)
37. M. Vallet, F. Bretenaker, A. Le Floch, R. Le Naour, M. Oger, The Malus Fabry–Perot interferometer. *Opt. Commun.* **168**, 423–443 (1999)
38. J. Morville, D. Romanini, Sensitive birefringence measurement in a high-finesse resonator using diode laser optical self-locking. *Appl. Phys. B* **74**, 495–501 (2002)
39. M. Durand, J. Morville, D. Romanini, Shot-noise-limited measurement of sub-parts-per-trillion birefringence phase shift in a high-finesse cavity. *Phys. Rev. A* **82**, 031803 (2010)
40. J.Y. Lee, H.-W. Lee, J.W. Kim, Y.S. Yoo, J.W. Hahn, Measurement of ultralow supermirror birefringence by use of the polarimetric differential cavity ringdown technique. *Appl. Opt.* **39**, 1941–1945 (2000)
41. H. Huang, *Noise Studies in CW Cavity Ring-Down Spectroscopy and Its Application in Trace Gas Detection* (Princeton University, Princeton, 2009)
42. P. Werle, R. Mücke, F. Slemr, The limits of signal averaging in atmospheric trace-gas monitoring by tunable diode-laser absorption spectroscopy (TDLAS). *Appl. Phys. B* **57**, 131–139 (1993)
43. Y. Wang, M. Nikodem, G. Wysocki, Cryogen-free heterodyne-enhanced mid-infrared Faraday rotation spectrometer. *Opt. Express* **21**, 740 (2013)
44. P. Kluczynski, S. Lundqvist, J. Westberg, O. Axner, Faraday rotation spectrometer with sub-second response time for detection of nitric oxide using a cw DFB quantum cascade laser at 5.33 μm . *Appl. Phys. B* **103**, 451–459 (2010)
45. D. Sofikitis, L. Bougas, G.E. Katsoprinakis, A.K. Spiliotis, B. Loppinet, T.P. Rakitzis, Evanescent-wave and ambient chiral sensing by signal-reversing cavity ringdown polarimetry. *Nature* **514**, 76–79 (2014)
46. L. Bougas, D. Sofikitis, G.E. Katsoprinakis, A.K. Spiliotis, P. Tzallas, B. Loppinet, T.P. Rakitzis, Chiral cavity ring down polarimetry: chirality and magnetometry measurements using signal reversals. *J. Chem. Phys.* **143**, 104202 (2015)